Comparison of near-infrared transmittance and reflectance measurements using dispersive and Fourier transform spectrophotometers

S. G. Kaplan, L. M. Hanssen, E. A. Early, M. E. Nadal and D. Allen

Abstract. A spectrophotometer based on an integrating sphere coupled to a commercial Fourier Transform Infrared (FTIR) instrument has been constructed for regular spectral transmittance and reflectance measurements over the 1 μm to 18 μm wavelength region. Despite the large number of sources of error that often limit the radiometric accuracy of FTIR measurements, we demonstrate uncertainties similar to established dispersive instrumentation. We performed near-normal-incidence reflectance and transmittance measurements on a series of samples over the 1 μm to 2.5 μm wavelength range using both FTIR and dispersive spectrophotometers. The results are compared, taking into account any differences in measurement geometry among the various systems and the combined measurement uncertainty. We find agreement within the combined uncertainties over most of the measured spectral region.

1. Introduction

Although there is extensive literature on the accuracy of regular (i.e. equivalent input and output geometry) spectral transmittance and reflectance measurements with both dispersive and FTIR spectrophotometers, there has been little direct comparison of data from the two types of system. In the ultraviolet, visible and near-infrared spectral regions, dispersive instruments will probably remain favoured for the highest-accuracy measurements at national standards laboratories. However, FTIR spectrometers have replaced dispersive instruments for thermal infrared measurements in many applications.

Despite the growing use of FTIR spectrophotometry in quantitative infrared measurements, where radiometric accuracy is very important, relatively little work has been done to quantify all the sources of uncertainty that contribute to a particular measurement result. Some effort has been made to catalogue and quantify the various sources of error in FTIR measurements [1, 2]. Comparisons have also been made of FTIR and laser-based transmittance measurements of neutral-density filters at 3.39 μm and 10.6 μm. However, these comparisons were limited to ultra-thin (approx. 100 nm thick) samples [2] in order to avoid etalon effects in the laser measurements.

S. G. Kaplan, L. M. Hanssen, E. A. Early, M. E. Nadal and D. Allen: Physics Laboratory, National Institute of Standards and Technology, Gaithersburg, MD 20899, USA.

A comparison of a more representative set of samples is needed to test the accuracy of the FTIR measurements on filters, mirrors or other optical components and materials that require calibration for use in radiometric applications. There are two dispersive instruments in the Optical Technology Division (OTD) at the National Institute of Standards and Technology (NIST) available for such comparisons: the Spectral Tri-Function Automated Reference Reflectometer (STARR), which performs specular, directional-directional, and directional-hemispherical reflectance measurements for the ultraviolet to near-infrared spectral regions [3], and the NIST Reference Spectrophotometer for Regular Spectral Transmittance [4], another monochromator-based system, which performs regular spectral transmittance measurements for the same spectral region. Both of these systems overlap with the FTIR-based system in the 1 μm to 2.5 μm wavelength region. Although this covers only a small region of the infrared, many of the sources of error in the measurements vary only gradually with wavelength. Thus the comparison can provide some indication of the accuracy of the FTIR system at longer wavelengths.

In this paper we present the results of transmittance measurements on four samples: a 5 mm thick silica-glass plate, a 2 mm thick absorbing glass filter, a 0.5 mm thick crystalline Si wafer, and a 0.25 mm thick Si wafer coated with NiCr. In addition, we measured the reflectance of a first-surface aluminium mirror and a black-glass sample. The differences between the dispersive and FTIR results are examined to see

whether or not they fall within the combined expanded uncertainty of the two measurements. We also consider any differences in beam geometry, polarization and spectral resolution among the various systems and estimate any differences in measured values that might result from these effects.

2. Experimental details

2.1 FTIR transmittance and reflectance measurements

The FTIR-based system uses a Bio-Rad FTS-60A FTIR spectrophotometer with external beam output as a source. For near-infrared measurements, the FTIR is configured with a quartz-tungsten-halogen (QTH) lamp and a TiO_2-coated quartz beam splitter. The nearly collimated output beam (approx. 50 mm diameter) from the FTIR is focused (f/4) on to an external variable aperture wheel, re-collimated, and directed into an integrating sphere with approximately f/6 focusing geometry. The entire system, including the integrating sphere, is housed in a sealed enclosure continuously purged with dry, CO_2-free air. The design and operation of the integrating sphere for transmittance and reflectance measurements has been described previously [5, 6]. Figure 1 shows the basic geometry of these measurements.

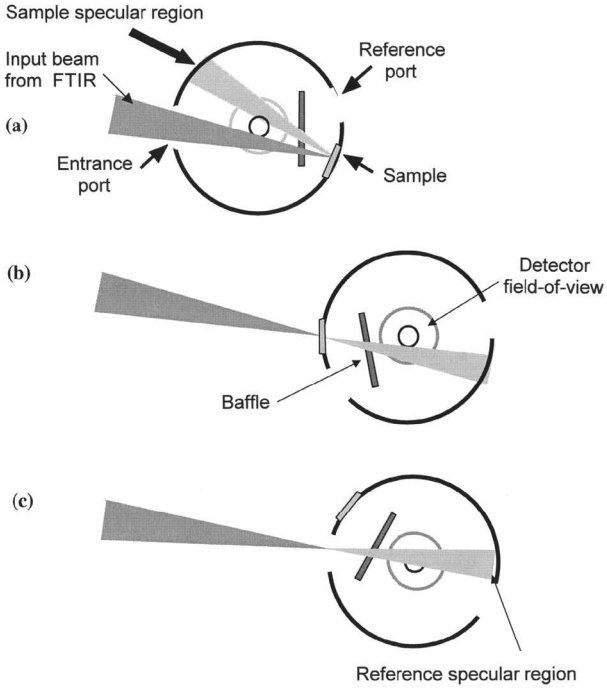

Figure 1. Geometry of integrating-sphere transmittance and reflectance measurements using an input beam from an FTIR spectrophotometer. (a) reflectance configuration: input beam reflects from sample at 8° and strikes sphere wall near entrance port; (b) transmittance configuration: beam passes through sample and strikes sphere wall in the same place as (a); (c) reference configuration: beam passes through reference port and strikes sphere wall on other side of entrance port.

The sample is mounted on the side of the sphere, and the detector (a liquid-nitrogen-cooled HgCdTe photoconductor) is mounted on the top, with its field-of-view restricted to a portion of the bottom of the sphere. The incident beam is focused at the sample position, and the sphere is rotated about both its centre and the entrance port to allow the beam to reflect from the sample front surface (Figure 1a), transmit through the sample (1b), or pass through the reference port (1c). In both the reflectance (a) and transmittance (b) configurations, the beam leaving the sample strikes a portion of the sphere wall next to the entrance port, which we designate the sample specular region, and is then scattered into the sphere volume. In the reference measurement (c), the incident beam strikes the sphere wall at a position on the other side of the entrance port to the sample specular region, known as the reference specular region. In an ideally manufactured sphere system, light incident on either the sample or reference specular regions would yield the same irradiance on the rest of the sphere wall. The ratio of the detected flux in the transmittance or reflectance position to that in the reference position yields an absolute transmittance or reflectance measurement of the sample. In practice, a small correction (approx. 0.2 %) is applied for throughput non-uniformity between the specular and reference regions, or the sample is measured in both the sample and reference ports and the results are averaged.

The advantages of the sphere for accurate transmittance and reflectance measurements have been discussed elsewhere [5]. The main feature is a reduced sensitivity to sample-induced geometrical changes in the beam incident on the detector. Although the sphere throughput is small (approx. 0.5 %), the multiplexing advantage of the FTIR allows data with adequate signal-to-noise and 8 cm^{-1} or 16 cm^{-1} resolution to be acquired in approximately 1 h to 3 h for samples with transmittance or reflectance between 0.01 and 0.99. The spectrometer and sphere positioning are computer-controlled. Typically, sample or reference spectra are acquired for several minutes each, and the process is repeated 20 to 30 times in order to average over drift in the FTIR signal level and estimate the repeatability component of the final measurement uncertainty.

The incident geometry at the sample position is nominally an f/5 or f/6 cone with its central axis at 8° to the sample normal; however, the central portion of the FTIR beam is blocked for use by the He-Ne alignment and position-sensing laser system in the interferometer. Thus, the range of incident angles excludes the central 1.5° or so (half-angle) of the cone. It is also possible to mount the sample on a compensating wedge to achieve normal incidence for the central (missing) rays; in this case a half-block is placed in the incident beam to remove interreflections between the sample and the FTIR. This was done for the absorbing glass filter described below to match more closely

the average absorption path length in the dispersive measurement. The spot diameter at the sample position is approximately 5 mm. The beam polarization has been checked using wire-grid polarizers and found to be quite small (Stokes components $s_2 \approx 0.03$ and $s_3 < 0.01$). Because of the 2π collection geometry of the side-mount sphere design, any scattered light from the exit side of the sample will be collected, unlike the two dispersive measurement systems described below. The diffuse component can be measured separately and subtracted if necessary, but all the samples used in this study are quite specular so that the diffuse component is negligible (less than 0.01 %).

For specular samples, a correction must be made to the measured transmittance or reflectance values to account for the light from the sphere wall that is back-reflected to the sample (Figures 1a or 1b) and lost out of the entrance port of the sphere. In the reference measurement (Figure 1c), the light back-reflected to the sample ends up striking the sphere wall and is not lost. The lost flux has been measured to be 0.25 % of the light reflected from the sample. The measured reflectance or transmittance is thus corrected by multiplying by $1 + 0.0025\ \boldsymbol{R}$, where $\boldsymbol{R}$ is the sample reflectance.

In addition to the repeatability (Type A) uncertainty component mentioned above, there are systematic (Type B) standard uncertainty components in the transmittance and reflectance measurements whose quadrature sum we have estimated to be approximately 0.1 % of the measured value at a given wavenumber. These estimates are based on analysis of the results of measurements on high-reflectance mirrors and transparent infrared materials [6], as well as an analysis of the sensitivity of the sphere throughput to system and sample alignment errors. The wavenumber scale of the instrument has been tested with high-resolution measurements of residual CO_2 and H_20 absorption lines in the purge gas and corrected to within 5 parts in 10^6. The linearity of the system response has been tested by using a series of apertures which vary the flux level reaching the sphere, without affecting the irradiation pattern on the detector, which is determined by its field-of-view limiting fore-optics. No evidence of non-linearity was found in the measured transmittance of a Si wafer over nearly two decades of flux level [7]. However, we have found small offset errors at short wavelength that may be related to interreflections or sampling errors within the FTIR spectrometer adding spurious features to the modulated signal. They are reduced by filtering out longer-wavelength light ($\lambda > 1.5$ μm) where necessary, but still may contribute an additional absolute Type B standard uncertainty component of 5 parts in 10^5. The expanded uncertainties in the FTIR measurements are calculated using the Type B relative uncertainty added in quadrature to the Type A component, which depends on the sample and averaging time, and multiplying the result by the coverage factor, $\boldsymbol{k = 2}$, for 95 % confidence intervals.

2.2 Dispersive transmittance measurements

Monochromator-based transmittance measurements were performed with the NIST Reference Spectrophotometer for Regular Spectral Transmittance. This instrument has undergone significant modifications for automation, but the optical design is similar to the one described previously [4]. Figure 2 shows the optical layout of this instrument.

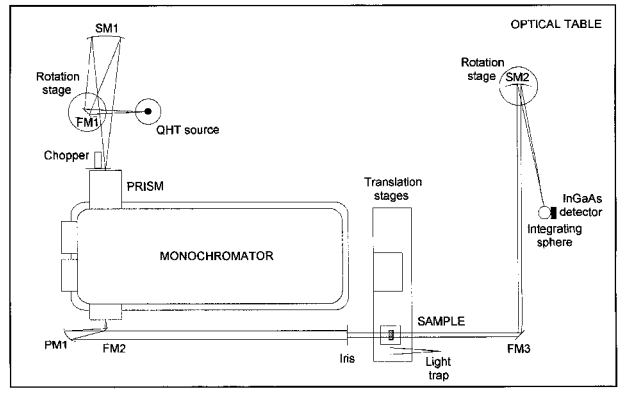

Figure 2. Optical layout of the NIST Reference Spectrophotometer for Regular Spectral Transmittance. For these measurements the source is a quartz-tungsten-halogen lamp and the detector is an extended-range InGaAs photoconductor. A translation stage sequentially places the open, sample, or light-trap position in the beam. The entire assembly is housed in a light-tight enclosure.

The instrument measures the transmittance of a sample using collimated, monochromatic radiant flux incident from the normal direction to the front surface of the sample. A spherical mirror focuses radiant flux from a QTH incandescent lamp through an optical chopper and on to the entrance slit of a prism-grating monochromator. The beam emerging from the exit slit of the monochromator is collimated by an off-axis parabolic mirror to within 0.1° and is incident on an iris to provide a circular incident beam. The beam passes through the sample carriage, is collected over a solid angle of 0.01 sr, and is focused by a spherical mirror into an averaging sphere. A signal proportional to the radiant flux of the beam is measured by an optical detector attached to the averaging sphere. The sample carriage consists of three incident positions for the beam: open, sample, and light trap. At each wavelength, signals are measured from the open, trap, sample, trap and open positions, in that order. Signals from the open and sample positions are proportional to the incident and transmitted fluxes, respectively. Net signals for the open and sample positions are obtained by subtracting the signals from the light trap position. The regular spectral transmittance of the test item is

given by the net sample signal divided by the average net open signal.

Individual samples were cleaned with an air bulb and mounted in a commercial lens holder with the beam centred on the front surface of the test item at normal incidence. This was achieved by adjusting tilts and translations of the sample holder and carriage until a laser beam at a wavelength of 632.8 nm, propagating collinear to the beam from the monochromator, was centred on the front of the test item and retroreflected.

The diameter of the incident beam was 10 mm. All samples were measured at wavelengths from 1000 nm to 2400 nm at increments between 10 nm and 25 nm with a 3 nm spectral bandwidth. The grating had 600 lines/mm and was blazed at 1250 nm; the detector was an InGaAs extended-range photodiode.

The three major components of uncertainty in measured transmittance values are the effects of wavelength error and detector non-linearity (Type B), and non-repeatability due to noise or drift (Type A). The wavelength uncertainty is 0.1 nm, which only contributes significantly to uncertainty on the transmittance scale near sharp attenuation features in the spectra, where the standard component can be as large as 0.0003 in some of the measurements reported here. The non-linearity uncertainty is a quadratic function of transmittance, with zero contribution at 0 or 1 on the transmittance scale, and a maximum of 0.000 25 at a transmittance of 0.5. The repeatability component is evaluated from the standard deviation of successive measurements. These three standard uncertainty components are added in quadrature over each wavelength band, and the result multiplied by a coverage factor of $k = 2$ to produce expanded uncertainty values for the dispersive transmittance measurements.

2.3 Dispersive reflectance measurements

Monochromator-based reflectance measurements were performed using STARR, which is designed to perform absolute spectral measurements of bidirectional, specular and directional-hemispherical reflectance [3]. Figure 3 shows the optical layout of this instrument. The source of radiant flux for STARR is a filter/grating-based monochromator, shown in the upper right of Figure 3a. For visible/near-infrared measurements, a QTH lamp was focused through a filter wheel and on to the entrance slit of the 0.25 m, f/3.9 monochromator, with a 600 line/mm grating blazed for 1000 nm. The entrance slit width was 2 mm, yielding a spectral resolution of 10 nm. Light exits the monochromator through a 1 mm diameter circular aperture, is collimated by a 51 mm diameter, 15° off-axis parabolic mirror, and directed to the rest of the system with a 51 mm flat mirror. The collimated beam has a diameter of approximately 14 mm and an angular divergence of less than 1°. For these measurements the incident angle at

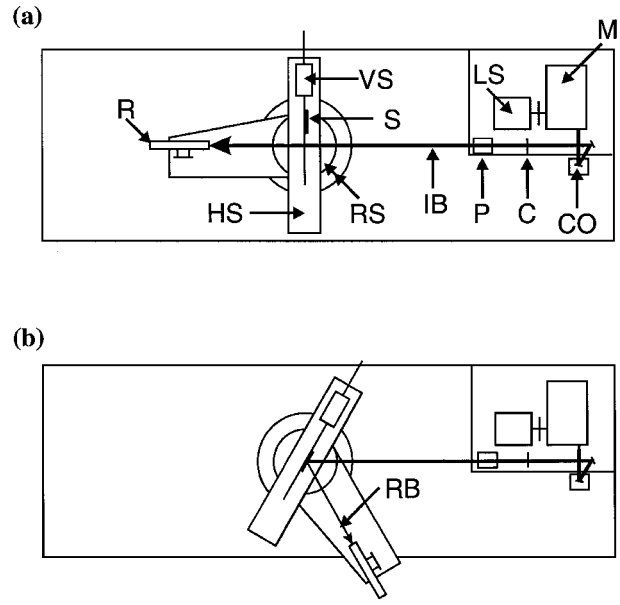

Figure 3. Schematic diagram of STARR showing the configuration for measuring (a) flux of incident beam and (b) flux of reflected beam. LS: light source; M: monochromator; CO: collimating optics; C: chopper; P: polarizer; IB: incident beam; S: sample; RS: rotation stages; VS: vertical stage; HS: horizontal stage; R: receiver; RB: reflected beam.

the sample position was 6° and the beam was nominally unpolarized.

Three detectors are manually interchangeable on the end of the receiver assembly mounted on the goniometer. For these measurements, a thermoelectrically cooled InGaAs photodiode mounted on a 38 mm diameter polytetrafluoroethylene (PTFE) integrating sphere was used. The incident beam was chopped and the detector signal measured with a phase-sensitive amplifier. Measured values of the reflected flux from the sample and straight-through flux from the source are ratioed to produce specular reflectance values at a series of wavelength settings of the monochromator, and the measurements are repeated to allow a statistical analysis. The entire system is located in a light-tight room with black walls, and computer-controlled from an adjoining room.

A detailed uncertainty analysis for measurements with this system is available [3]. In the measurements reported here, the dominant sources of uncertainty are incident angle, sample uniformity and detector noise, and the expanded uncertainty is approximately 0.0012 on the reflectance scale.

2.4 Samples

For this comparison, four samples were selected for transmittance and two for reflectance measurements. The chief criteria were uniformity, specularity and relative insensitivity to incident beam geometry, in order to minimize the need for correction factors due

to different incident angles and optical path lengths in the materials. We also wanted to test both large (near 1) and small (<0.1) values on the radiometric scale to assess linearity. All six samples were measured on the FTIR system described in Section 2.1, while the monochromator-based measurements were performed on one of the systems in Sections 2.2 and 2.3. All three facilities are kept in rooms fitted with air-filtration units to reduce particulate accumulation. The room temperatures did not vary outside the range 22 °C to 24 °C.

The transmittance samples were a 5 mm thick 25 mm diameter fused-silica plate from VLOC Corporation (actually an uncoated etalon), a 2 mm thick 25 mm diameter absorbing glass filter from Reynard Corporation, designed as a 10 % neutral-density filter for visible wavelengths, a <100>-oriented 0.5 mm thick 25 mm diameter high-resistivity (>20 Ω cm) Si wafer from Virginia Semiconductor, and a nominally 1 % neutral density NiCr coating for 2 μm to 4 μm from Spectrogon, Inc., on a 0.25 mm thick Si substrate. For the reflectance measurements, the samples were 51 mm diameter mirrors: a first-surface aluminium mirror (NIST Standard Reference Material (SRM) 2003), and a black-glass sample similar to SRM 2026. Neither of these samples has a significant contribution from the back-surface reflection.

3. Results and discussion

3.1 Transmittance

Figure 4a shows the measured regular spectral transmittance for the fused-silica plate with the FTIR and monochromator-based systems, while the difference between the two measurement results is shown in Figure 4b. Over most of the spectral region, the difference between the two measurements is less than the combined uncertainty (calculated as the quadrature sum of the $k = 2$ expanded uncertainties of each measurement result) shown by the solid curves. The differences are largest near the fused-silica absorption features at 1.4 μm and 2.2 μm, with one outlier point on the steep edge of the absorption line at 2.2 μm probably due to a difference between the effective spectral resolutions of the two systems. The difference of 0.008 is more than an order of magnitude larger than would be expected from the combined wavelength uncertainties in the two instruments. Increased noise is seen in the H_2O vapour absorption region around 1.85 μm. The uncertainty in the FTIR data grows at shorter wavelengths due to the reduction in modulated signal level and interferometric stability.

For this measurement, the FTIR data were taken with an average angle of incidence of 8° and an f/5 cone, while the monochromator data were taken at near normal incidence and collimated. In the transparent spectral regions of fused silica, the difference between

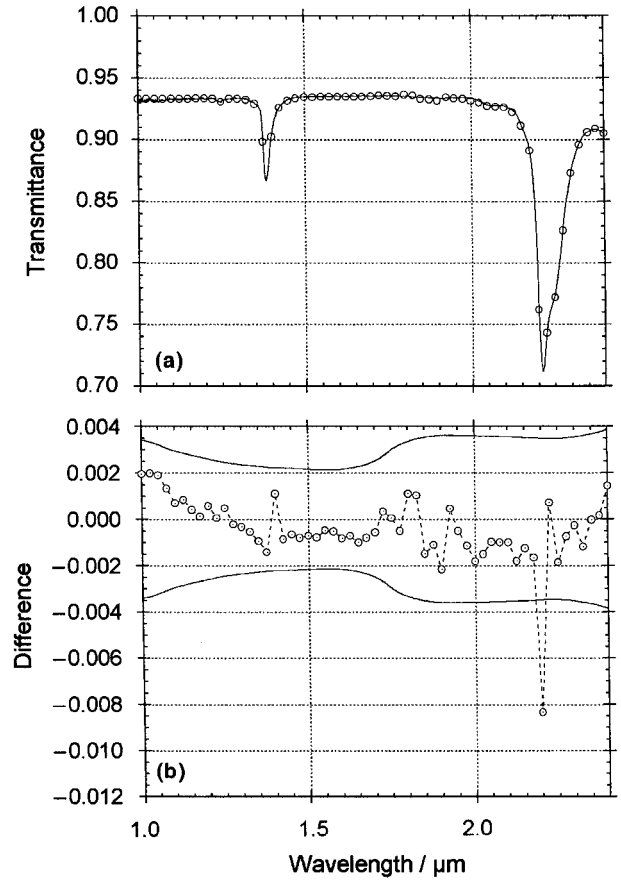

Figure 4. Comparison of FTIR and monochromator measurements of 5 mm thick fused-silica transmittance. (a) measured transmittances, with open circles showing monochromator data and solid curve showing FTIR data; (b) difference $(T_{\mathrm{mono}} - T_{\mathrm{FTIR}})$ between the two measurement results (open circles) and combined uncertainty $(k = 2)$ in the two measurements (solid curves).

the measured values in these two geometries for unpolarized light is expected to be less than 0.0001. At the minimum transmittance value of about 0.71 near 2.2 μm, the FTIR data are expected to be roughly 0.001 lower than the monochromator results because of the increased absorption path length in the material. This effect is not resolvable in the data shown in Figure 4b.

The second sample that was compared in transmittance was the 2 mm thick absorbing-glass filter. The results of these measurements are shown in Figure 5a, while Figure 5b shows the difference between the two sets of data. This sample has much lower transmittance than the fused silica and thus provides a test of the linearity of both systems. Over the 1.3 μm to 2.4 μm wavelength range, the differences between the two sets of data are mostly within the combined expanded uncertainty $(k = 2)$ of the two measurements. At shorter wavelengths (less than 1.3 μm), the differences grow systematically larger outside the expected statistical fluctuations, with the FTIR data consistently higher than the monochromator data. Near the minimum in transmittance of about 0.08

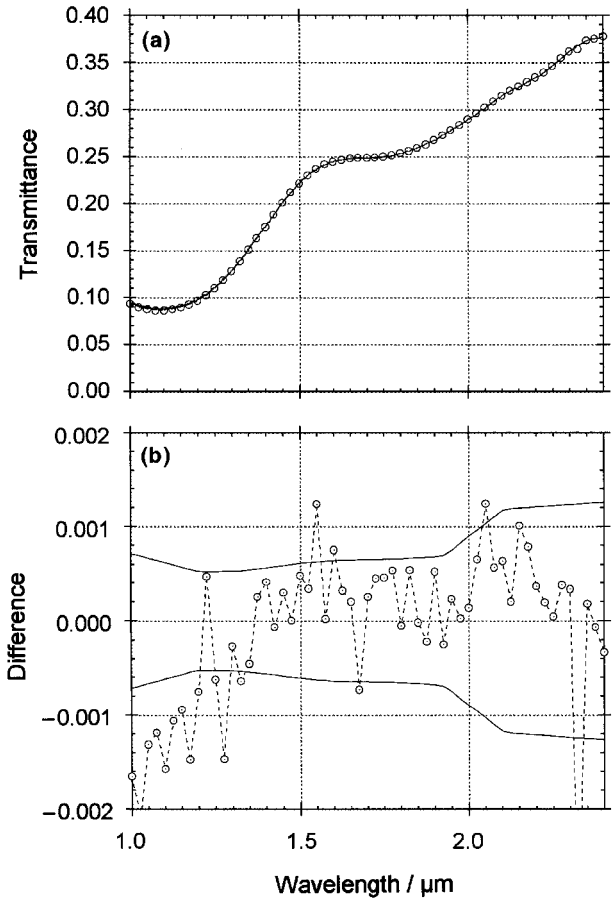

Figure 5. Comparison of FTIR and monochromator measurements of a 2 mm thick absorbing-glass filter. (a) measured transmittances, with open circles showing monochromator data and solid curve showing FTIR data; (b) difference $(T_{\mathrm{mono}} - T_{\mathrm{FTIR}})$ between the two measurement results (open circles) and combined uncertainty $(k = 2)$ in the two measurements (solid curves).

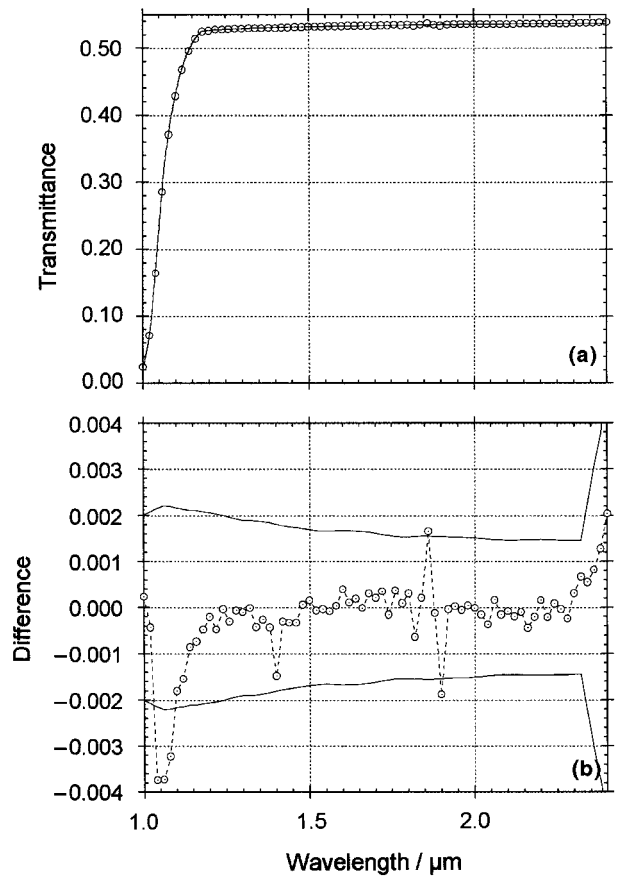

Figure 6. Comparison of FTIR and monochromator measurements of a 0.5 mm thick Si wafer. (a) measured transmittances, with open circles showing monochromator data and solid curve showing FTIR data; (b) difference $(T_{\mathrm{mono}} - T_{\mathrm{FTIR}})$ between the two measurement results (open circles) and combined uncertainty $(k = 2)$ in the two measurements (solid curves).

at 1.1 μm, the FTIR value would be expected to be 0.0024 lower than the monochromator value due to the increased path length of the converging beam. However, the observed difference is less than 0.002 and has the opposite sign to what is expected. The differences between the two sets of data at these short wavelengths could be caused by spurious harmonic signals in the FTIR spectrum, which need to be investigated more closely.

Figure 6a shows the transmittance comparison for a 0.5 mm thick Si wafer, with the difference between the monochromator and FTIR data shown in Figure 6b. Over most of the spectral region, the differences are less than 0.001 and thus smaller than the combined uncertainty of the two measurements. The difference in measured values due to variation in beam geometry between the two systems is expected to be smaller than the combined measurement uncertainty. In the transparent spectral region for Si ($\lambda > 1.5$ μm) the difference due to the 8° incident, f/6 geometry of the sphere is at most expected to be 0.0001 for the nearly unpolarized beam. Near the cutoff wavelength at 1 μm, the expected decrease in transmittance due to the increased path length in the sphere geometry is only 4×10^{-5}, significantly smaller than the combined measurement uncertainty.

The sharp structures apparent at 1.4 μm and 1.85 μm in Figure 6b may result from H_2O vapour absorption. They appear mostly in the monochromator data, which were not acquired under purged conditions. The difference grows systematically larger, reaching –0.004 at the Si absorption edge near 1.1 μm. The possibility was considered that this discrepancy arises from an error in wavelength in one or both instruments, but the differences are too large and the average amplitude cannot be made any smaller by shifting the abscissa scale of one data set relative to the other. At the short-wavelength limit of the data, the FTIR data were measured using a 8000 cm^{-1} to 12 000 cm^{-1} bandpass filter in order to reduce any effect of false harmonic signals from interreflections or sampling errors, which can be significant for high-frequency measurements at low levels of signal. Some of the discrepancy between

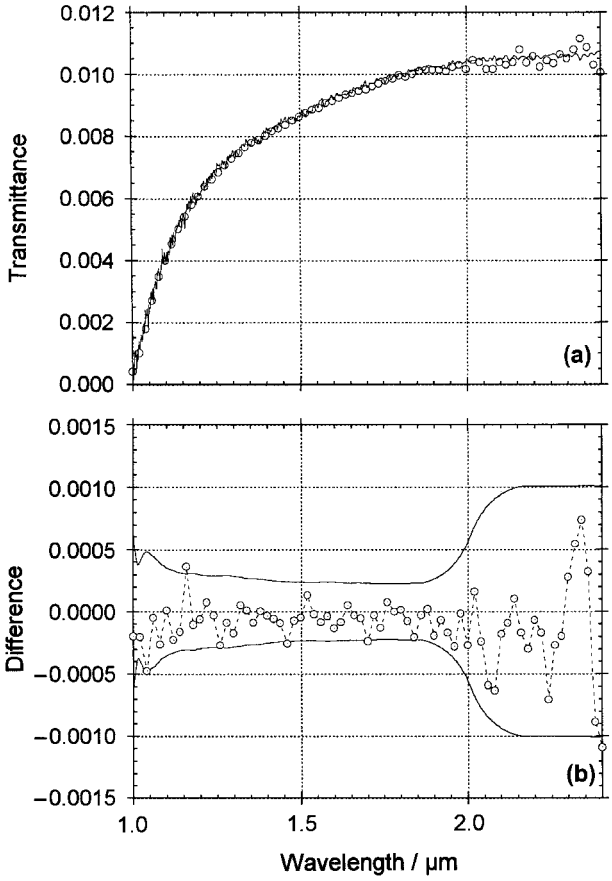

Figure 7. Comparison of FTIR and monochromator measurements of a 0.25 mm thick Si wafer with a NiCr coating. (a) measured transmittances, with open circles showing monochromator data and solid curve showing FTIR data; (b) difference $(T_{\mathrm{mono}} - T_{\mathrm{FTIR}})$ between the two measurement results (open circles) and combined uncertainty $(k = 2)$ in the two measurements (solid curves).

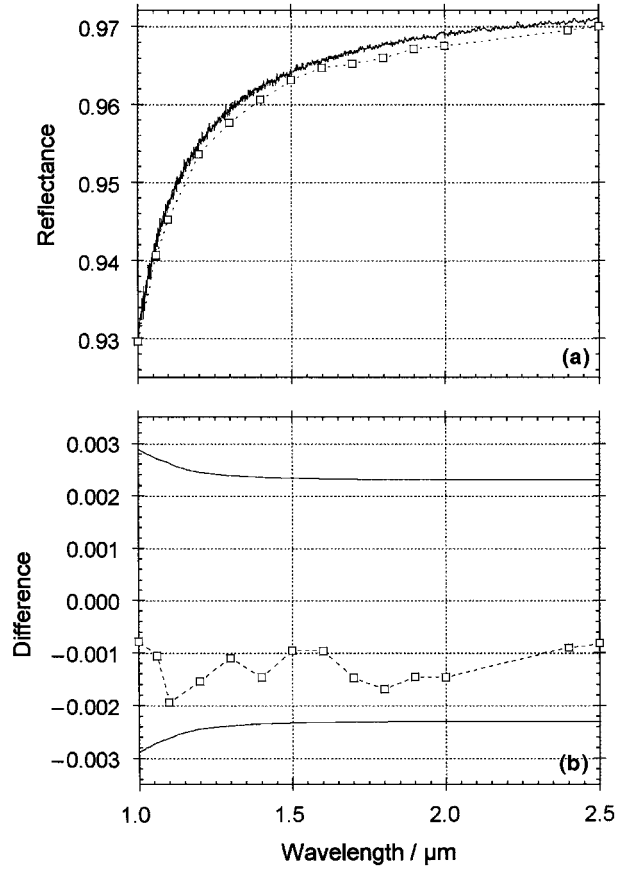

Figure 8. Comparison of FTIR and STARR reflectance measurements of an SRM 2003 aluminium mirror. (a) measured reflectances with STARR as open squares and FTIR as solid line; (b) difference $(R_{\mathrm{STARR}} - R_{\mathrm{FTIR}})$ between the two measurements (squares) and combined uncertainty $(k = 2$, solid lines).

the FTIR and monochromator results may be attributed to residual harmonics in the FTIR measurement, but some may also result from differences in effective resolution between the two systems. These differences need to be investigated more closely.

The final sample to be compared in transmittance was the 0.25 mm thick Si with NiCr coating, shown in Figure 7. The difference between the transmittances measured at normal incidence and 8° f/6 geometry for this sample, consisting of an absorbing metallic film on an absorbing substrate, is expected to be of order 1×10^{-5} or smaller, much less than the combined measurement uncertainty. The difference between the two measurement results, shown in Figure 7b, is on average about 1×10^{-4}, with the FTIR measurement being higher than the monochromator result. However, the observed differences are less than the combined uncertainty for most of the wavelengths measured.

3.2 Reflectance

Figure 8 shows a comparison of reflectance measurements at 8° (FTIR) and 6° (STARR) on an SRM 2003 Al mirror. As may be seen, the agreement at all wavelengths is well within the combined uncertainty for the two measurements, with the FTIR values consistently about 0.001 higher than the STARR values. We do not believe that this difference results from non-uniformity of the sample, although the spot diameters on the sample were quite different (5 mm versus 14 mm). Because both beams are nearly unpolarized, the difference due to incident angle should be negligible (approx. 3×10^{-5}). Further comparisons of high-reflectance mirrors may reveal a systematic difference between the two systems that would be interesting to investigate.

Finally, Figure 9 shows a comparison of the FTIR and STARR measurements on the black-glass sample. This sample has a reflectance of approximately 0.04 over the measured spectral range, and again the two measurements agree within the combined uncertainty. Much of the uncertainty comes from non-uniformity

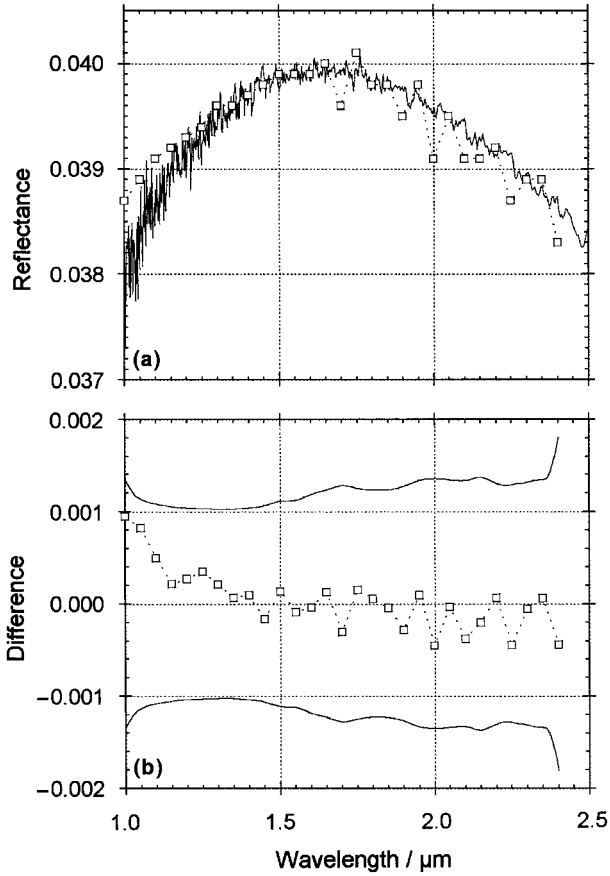

Figure 9. Comparison of FTIR and STARR reflectance measurements of a black-glass mirror. (a) measured reflectances with STARR as open squares and FTIR as solid line; (b) difference $(R_{\mathrm{STARR}} - R_{\mathrm{FTIR}})$ between the two measurements (squares) and combined uncertainty ($k = 2$, solid lines).

in the black glass. The average difference is much less than the expanded uncertainty $(k = 2)$, indicating that the uniformity near the centre of the sample may be somewhat better. An apparently systematic difference between the two measurements can be seen between 1 μm and 1.3 μm. This is the same region where the differences in transmittance were noted in the absorbing-glass filter (Figure 5b). The discrepancy again points to the possibility of small spurious modulation errors in the FTIR measurement that become significant in the spectral regions where the level of flux is small compared with the peak value.

4. Conclusions

A comparison has been made of near-normal regular transmittance and specular reflectance measurements of a series of samples on FTIR and monochromator-based spectrophotometers. We find agreement within the combined expanded uncertainty of about 0.002 $(k = 2)$ over most of the measured spectral range, and an ordinate scale range of nearly three decades. The only indication of systematic differences outside the combined uncertainties is found at the short-wavelength limit of the data, most prominently in Figures 5 and 6. We are currently investigating the possibility of interreflection or sampling errors in the FTIR spectrometer affecting the measurement results near the short-wavelength cutoff of 1 μm, where the overall signal is low compared with that at longer wavelengths, and residual false harmonic features could be significant sources of error in the sample/reference ratios. We will also be adding an InSb detector to the sphere system to increase the signal-to-noise ratio in the near-infrared region and improve our evaluation of the measurement uncertainties in this spectral region.

Note. The mention of certain trade names in this manuscript is for information only and not meant to imply an endorsement by the National Institute of Standards and Technology or that the equipment mentioned is necessarily the best suited for the task.

References

1. Birch J. R., Clarke F. J. J., *Spectroscopy Europe*, 1995, **7**, 16-22.
2. Kaplan S. G., Hanssen L. M., Datla R. U., *Appl. Opt.*, 1997, **36**, 8896-8908.
3. Barnes P. Y., Early E. A., Parr A. C., *Natl. Inst. Stand. Technol. Spec. Publ. 250-48*, Washington, D.C., U.S. Government Printing Office, 1998.
4. Eckerle K. L., Hsia J. J., Mielenz K. D., Weidner V. R., *Natl. Bur. Stand. Spec. Publ. 250-6*, Washington, D.C., U.S. Government Printing Office, 1987.
5. Hanssen L., Kaplan S., *Proc. SPIE*, 1998, **3425**, 16-27.
6. Hanssen L. M., *Appl. Opt.*, 2001, **40**, 3196.
7. Hanssen L. M., Kaplan S. G., *Vibr. Spect.*, 2001, in press.

Received on 5 December 2001 and in revised form on 31 January 2002.